

Article

Thermal and Catalytic Pyrolysis of Urban Plastic Waste: Modified Mordenite and ZSM-5 Zeolites

Taihana Parente Paula ¹, Maria de Fatima Vieira Marques ^{1,*}, Mônica Regina da Costa Marques ², Michelle Souza Oliveira ³ and Sergio Neves Monteiro ³

¹ Instituto de Macromoleculas Professor Eloisa Mano, Universidade Federal do Rio de Janeiro, Horácio Macedo Av., 2.030, Bloco J, Cidade Universitária, Rio de Janeiro CEP 21941-598, RJ, Brazil; taihana.parente@gmail.com

² Institute of Chemistry, State University of Rio de Janeiro, St. São Francisco Xavier, 524, Pavilhão Haroldo Lisboa da Cunha, Maracanã, Rio de Janeiro CEP 20550-0900, RJ, Brazil; monicamarquesuerj@gmail.com

³ Department of Materials Science, Military Institute of Engineering, IME, Praça General Tibúrcio, 80, Urca, Rio de Janeiro CEP 22290-270, RJ, Brazil; oliveirasmichelle@ime.eb.br (M.S.O.); snevesmonteiro@gmail.com (S.N.M.)

* Correspondence: fmarques@ima.ufrj.br



Citation: Paula, T.P.; Marques, M.d.F.V.; Marques, M.R.d.C.; Oliveira, M.S.; Monteiro, S.N. Thermal and Catalytic Pyrolysis of Urban Plastic Waste: Modified Mordenite and ZSM-5 Zeolites. *Chemistry* **2022**, *4*, 297–315. <https://doi.org/10.3390/chemistry4020023>

Academic Editors: Vincenzo Vaiano and Olga Sacco

Received: 26 January 2022

Accepted: 30 March 2022

Published: 8 April 2022

Publisher's Note: MDPI stays neutral with regard to jurisdictional claims in published maps and institutional affiliations.



Copyright: © 2022 by the authors. Licensee MDPI, Basel, Switzerland. This article is an open access article distributed under the terms and conditions of the Creative Commons Attribution (CC BY) license (<https://creativecommons.org/licenses/by/4.0/>).

Abstract: Zeolites have been successfully applied as catalysts in the pyrolysis of plastics to obtain valuable lower molecular weight hydrocarbon compounds. In the present work, mordenite was directly synthesized and chemically modified from commercial mordenite to increase pore volume. For the first time, the performance of these mordenites was compared with that of an alkali-treated ZSM-5 as catalysts for assisting the pyrolysis of simulated urban plastic waste. The investigated zeolites were: (i) as-supplied synthetic ZSM-5 (ZSM-5/AS); (ii) 0.2 M NaOH treated ZSM-5 (ZSM-5/02); (iii) as-supplied mordenite (MOR/AS); (iv) 0.2 M NaOH treated mordenite (MOR/02); and (v) synthetic lab-developed mordenite (MOR/SD). The modified and synthesized zeolites were individually applied as catalysts in the 700 °C pyrolyzes of combined polyethylene, polypropylene, and polystyrene wastes in a mixture simulating most plastics found in Rio de Janeiro (Brazil) city garbage composition. X-ray diffraction revealed crystallite sizes of all zeolites in a nanometric range from 17 to 43 nm. Textural analysis disclosed the alkali-treated ZSM-5/02 with a superior external surface area, 153 m²/g, and mesopore volume equal to 0.253 cm³/g. Lower values were obtained by MOR/02 (39 m²/g and 0.072 cm³/g). The pyrolysis of the plastic mixture with ZSM-5/02 presented a lower initial degradation temperature, 387 °C, followed by MOR/02, with 417 °C. The ZSM-5/02 catalyst obtained the highest conversion in the pyrolysis of the plastic mixture, totaling 49.2%. However, pyrolysis assisted by the MOR/02 catalyst showed the largest fraction (81.5%) of light hydrocarbons.

Keywords: catalyst; zeolites; mordenite; ZSM-5; pyrolysis; plastic waste

1. Introduction

Plastic production has faced exponential growth in recent decades, as shown in Figure 1 [1], since its use became widespread in the 1950s, keeping up with global financial growth. This growing demand and consumption of plastics generated large amounts of waste, resulting in socioeconomic and environmental problems [2]. It is estimated that plastic waste increases at rate of 3.9% per year [3]. This, combined with other solid waste, turns plastic waste management into an overwhelming problem. Geyer et al. [4] estimated that if waste production increases, approximately 12 trillion tons of plastic waste will pollute water bodies and exhaust landfills by 2050.

Disposal in landfills and incineration for energy production is still the most common method of eliminating plastic waste. In general, solid waste management presents a challenge, but it can be seen as an opportunity to obtain other goods such as mechanically

recycled by-products, heat, or energy [5]. Indeed, there is a growing interest in alternatives to fossil fuels with waste-derived raw materials, such as biomass from agroindustry residues and plastic wastes. The latter receives the most attention mainly due to their impact and environmental benefits [3,5–7].

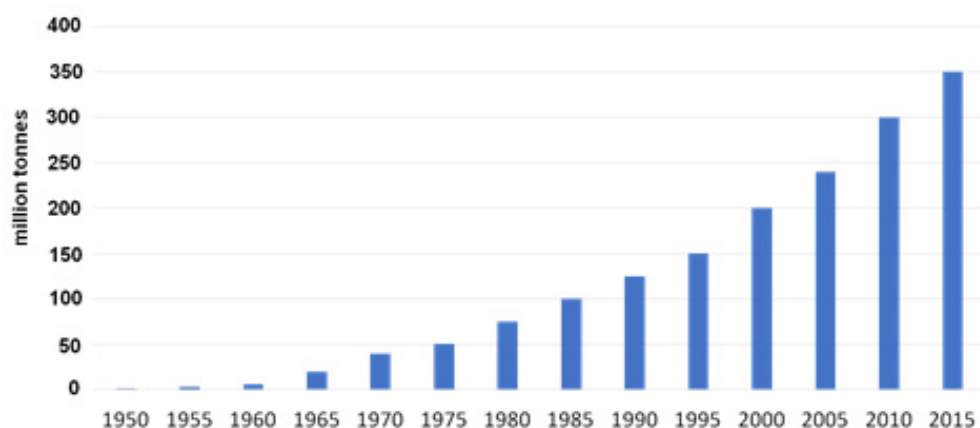


Figure 1. Evolution of global plastics production annually.

Thermochemical conversion technologies have gained increasing attention to plastic waste management. Compared with combustion, pyrolysis has significant advantages since it produces low amounts of gaseous pollutants due to the absence of oxygen in the process [3]. The composition of specific elements of residual plastics inspires researchers to seek alternative recovery technologies to produce highly valuable chemicals and fuels from post-consumer plastics rather than simple incineration [6,8]. In this scenario, pyrolysis has become a promising alternative since its main product is wax/oil, a substitute for heavy fuel. It might also be applied as a raw material for the petrochemical industry [9]. Together with the production of coal and gases, it can be sold later to add value to the global process [3].

Catalytic assisted pyrolysis has the advantage of allowing the control of the composition and distribution of compounds obtained, with a lower energy consumption of the process and greater selectivity for valuable chemicals [10]. Zeolites are widely used as catalysts in the degradation of polymers due to their strong acidity, which favors the rupture of the carbon–carbon bond [11]. ZSM-5 stands out owing to its marked selectivity in the formation of branched hydrocarbons fostered by isomerization and aromatization reactions as a function of the zeolitic structure, including acid strength, external specific area, and microporosity [12,13]. ZSM-5 zeolite is formed by pentasil units in a three-dimensional micropore system consisting of two 10-member rings perpendicularly interconnected, straight channels with dimensions of 0.55×0.51 nm and zigzag channels 0.56×0.53 nm. These dimensions characterize ZSM-5 as a zeolite of intermediate or medium-sized pores [14]. In addition, ZSM-5 has a stereo impedance of interconnectivity, limiting mass transfer in its pores, making the depolymerization process more difficult. These mass transfer limitations are less evident in mesoporous materials [15].

Santos et al. [16], when studying chemical treatments for PE and PP pyrolysis, showed that the alkaline treatment in ZSM-5 zeolites effectively produced mesopores and increased light production fractions in pyrolysis products when compared to the same zeolite without treatment. By contrast, the mordenite is a zeolite with a typical composition of $\text{Na}_8\text{Al}_8\text{Si}_{40}\text{O}_{96} \cdot 24\text{H}_2\text{O}$ and orthorhombic symmetry [17]. Its porous structure consists of two types of pores. The first is a one-dimensional system that features an opening with 12-member rings, with the main dimension of 0.65×0.70 nm. The second is a tortuous system with rings of 8 members, perpendicular to the first, with a dimension of 0.26×0.57 nm, forming the so-called side pockets [18]. The dimensionality of the mordenite channel structure (1D/2D vs. 3D in MFI structure) makes it difficult for large molecules to diffuse and

allows the diffusion of only small molecules such as nitrogen and oxygen gases through their pores. The opening space of tortuous pores does not allow the entrance of larger molecules, as in the case of organic macromolecules, which can only spread in a system of pores with relatively larger opening spaces by unilateral diffusion [19,20]. The main drawback of mordenite is its limited size of channels and cavities, including the lack of interconnectivity. Therefore, it imposes diffusion limitations on reactions, especially in giant molecules, such as high molecular weight polymers [19,21]. Because of this, the mordenite becomes more susceptible to the deactivation of pores by the deposition of the residual coke carbon or solid fraction originated in the pyrolysis [21–23]. The diffusion problem of larger molecules can be overcome by employing zeolites with small crystal sizes and high specific areas [8]. Therefore, to take advantage of the good properties of this zeolite, it is very important to study new syntheses and chemical modifications in the mordenite to increase its porosity and promote the interconnectivity of its channels.

This research aims to develop new pyrolysis catalysts to recycle plastic waste, comparing its performance with a reference zeolite ZSM-5 to convert it into new valuable hydrocarbons. Alkaline treatment is indicated as an effective way for the formation of mesopores. This treatment can preserve its acidity with a selective desilication of zeolite [11,21]. The mordenite with mesoporous structure is still scarcely reported in the literature for such application. Thus, for the first time, a comparative study of chemically-modified (MOR/02) and synthetic-developed (MOR/SD) mordenites with alkali-modified ZSM-5 was conducted in the pyrolysis of a plastic waste mixture. The mixture of plastics was based on the data of polymer resins most consumed in Brazil [24], as a method to simulate urban waste, formed only by commodity plastics, that is, polyethylene (PE), polypropylene (PP), and polystyrene (PS) in concentrations equivalent to those typically found in urban garbage landfills.

2. Results

2.1. Catalyst Characterization

Table 1 shows the bulk (Si/Al_{bulk}), surface (Si/Al_{bulk surface}), framework (Si/Al_{framework}), and EFAL composition of the studied zeolites, expressed as molar ratio obtained via ED-XRF, EDS, and ²⁹Si MAS NMR, respectively. The amount of EFAL was determined by ²⁷Al MAS NMR. The NMR spectra are presented in Supporting Information (Figures S1–S6).

Table 1. Bulk, bulk surface, framework Si/Al molar ratio, and EFAL content of the studied zeolites.

Sample	Si/Al _{bulk} ^a	Si/Al _{bulk surface} ^b	Si/Al _{framework} ^c	EFAL ^d (%)
MOR/AS	6.6	4.5	-	-
MOR/02	6.5	5.9	8.4	26.8
MOR/SD	8.7	5.4	9.9	24.3
ZSM-5/AS	13.4	n.d.	-	-
ZSM-5/02	12.5	10.3	16.0	18.8

^a ED-XRF, ^b EDS, ^c ²⁹Si MAS NMR, ^d ²⁷Al MAS NMR; EFAL = extra-framework Al; n.d.—not determined.

The removal of Si by alkaline treatment proved to be more efficient for a ZSM-5 zeolite, in not detecting a significant decrease concerning Si/Al for a mordenite. However, ²⁹Si and ²⁷Al MAS NMR analyses reveal how the changes occurred by these post-treatments [25]. The MOR/02 leaching process led to a slight decrease in Si (0Al) peak intensity and a higher EFAL (26.8%). This result can be justified since, during desilication, Si species not linked to Al, Si (⁰Al), can be easily leached.

However, it is difficult to remove Si atoms in Si (¹Al) because the negatively charged AlO₄ tetrahedron makes hydrolysis of the Si–O–Al bond in alkaline solution difficult [26]. For zeolite ZSM-5/02, there was a slight decrease in Si/Al ratio (~6%) compared to the starting ZSM-5/AS sample. For the synthesized mordenite, MOR/SD, a higher Si/Al ratio was obtained than the alkali-treated MOR/02 mordenite, which was also confirmed by NMR analysis.

For all mordenite materials in this study, it was observed that the octahedral Al showed a greater signal than expected, close to 0.9 ppm. Therefore, it is speculated that the alumina clusters causing the chemical shift (close to 0.5 ppm) are located on the outer surface of zeolite crystals [27].

Additionally, a transitional peak was observed in all samples between the two main peaks of the ^{27}Al MAS NMR spectrum and between tetrahedral Al and octahedral Al, located as a shoulder after the peak at 50 ppm. This peak is attributed to distorted tetrahedral Al (IV) or pentacoordinate Al species probably associated with structural Al atoms, disturbed by less orderly environments of mesoporous samples [28]. This disorder in the crystalline structure of the zeolite, with the formation of extraframework Al species, would be responsible for the gradual amorphization of the observed structure, intensified with the alkaline treatment, resulting in a decrease of crystallinity shown by the lower peak intensity and increased peak base in the XRD diffractogram, shown in Figure 2. The position and intensity of observed peaks were compared with the standard diffractograms in the literature (Database of zeolite Structure) (Figure S7 in Supporting Information).

To quantify this structural modification resulting from the alkaline treatment, the XRD of the samples was performed (Figure 2), in which it was possible to calculate the degree of crystallinity of the treated samples by the ratio between the areas of all diffraction peaks for the modified samples and the starting structure corresponding areas of the as-supplied untreated zeolites, the latter chosen as reference [25].

The results of the degree of crystallinity are displayed in Table 2. The results showed that the crystallinity of the MOR/02 sample was 95.1%, confirming that the leaching process decreased the crystallinity degree of these zeolites. Concerning ZSM-5/02, characteristic peaks of the little affected structure were obtained with crystallinity estimated close to 97% compared to the as-supplied ZSM-5/AS zeolite. The obtained result agrees with other studies [14,28], which found that the relative crystallinity of zeolites treated with NaOH solution between 0.1–0.2 mol/L was not affected by desilication.

Table 2. Size of the crystallite (D) calculated by the Scherrer equation.

Sample	2θ (°)	β (FWHM)	D (nm)	Crystallinity (%)
MOR/AS	25.71	0.2000	42.9	100
MOR/02	25.84	0.2338	34.8	95.1
MOR/SD	25.98	0.2294	35.6	-
ZSM-5/AS	23.39	0.4799	16.9	
	8.18	0.2618	30.4	100
ZSM-5/02	23.18	0.4499	18.0	
	7.96	0.2393	33.3	97

Another very important piece of data extracted from the XRD was crystallite size. The dimensions of zeolite crystallites have important implications for the diffusion rates of molecules within its structure, as well as the contribution of the external surface area. The size of the crystallites (D) of the catalysts was determined by the Scherrer equation.

Table 2 correlates the D values using the most intense peak corresponding to the crystallographic plane (060) for mordenite, as in the literature [29].

The crystallite size of the ZSM-5 zeolites was calculated by considering the interplanar distance of 1.115 nm ($2\theta = 7.8^\circ$) and 1.005 nm ($2\theta = 8.5^\circ$), which in the literature [30,31] correspond to the most intense peaks. For the samples synthesized in this work, the most intense peaks were those with interplanar distances of 0.384 nm ($2\theta = 23.18^\circ$) and 0.382 nm ($2\theta = 23.39^\circ$) [32,33] concerning the crystallographic planes (101) and (501), respectively. For the as-supplied MOR/AS mordenite, alkaline desilication produced material with smaller crystallite sizes with alkali concentration, while ZSM-5 was little affected by desilication.

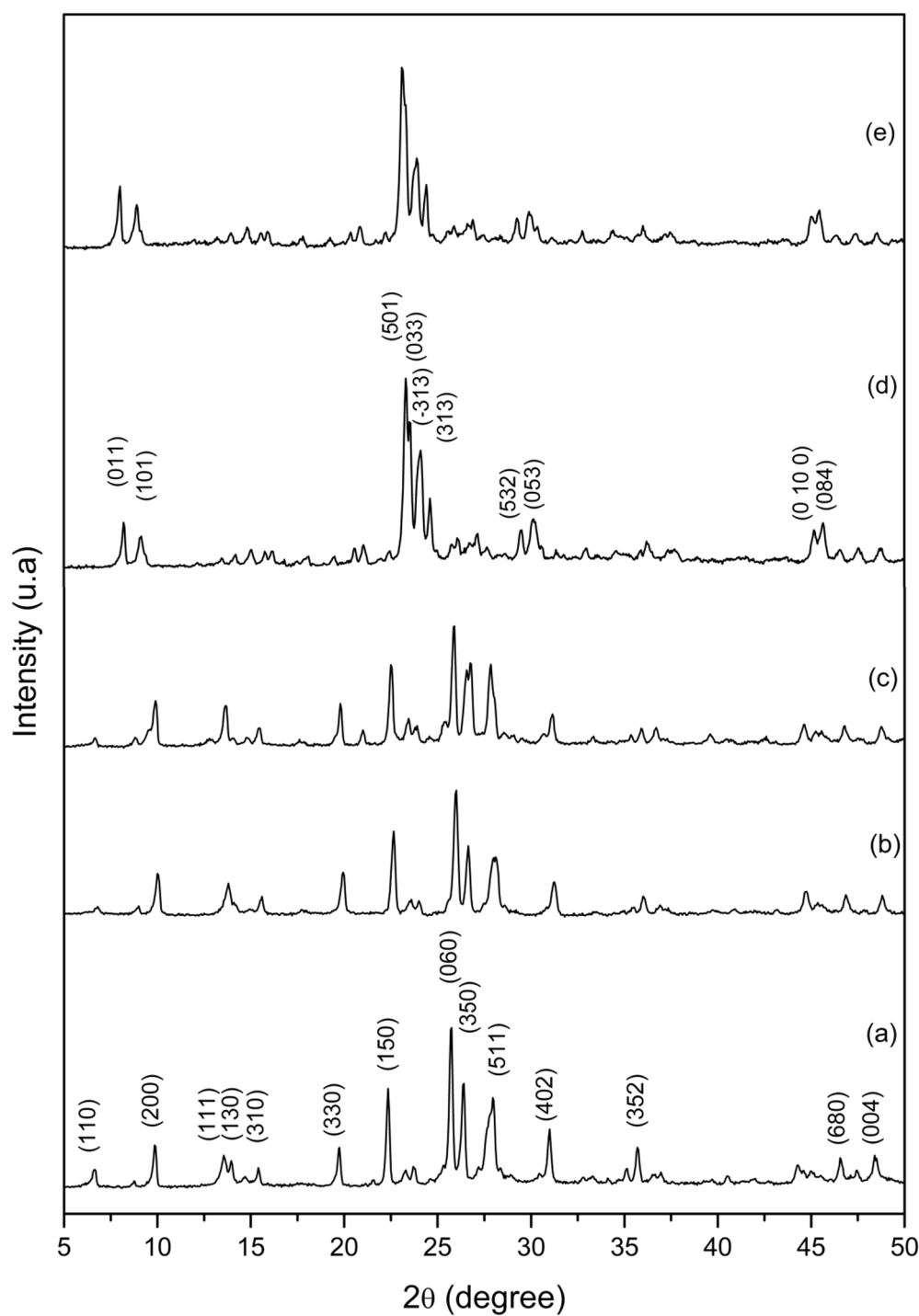


Figure 2. XRD patterns of (a) MOR/AS, (b) MOR/02, (c) MOR/SD, (d) ZSM-5/AS, (e) ZSM-5/02.

The isotherms of the sample obtained from MOR/02 display a profile very close to that reported by Bertrand-Drira et al. [34], with a step in P/P_0 close to 0.5 in the desorption branch. This behavior was justified as a typical capillary condensation phenomenon, indicating that some mesopores were connected to the crystal surface. In addition, the isotherms showed marked adsorption at low relative pressures, revealing the preservation of microporosity.

All mordenite showed H4 type hysteresis, which does not limit adsorption at high relative pressures. This hysteresis type indicates that MOR catalysts do not have well-defined mesoporous structures with wide pore size distribution [35]. For the synthetic-

developed mordenite MOR/SD, 17% of mesopores were obtained concerning the total pore volume. For the synthetically-developed mordenite MOR/SD, 17% of the mesopores were obtained (Figure 3a).

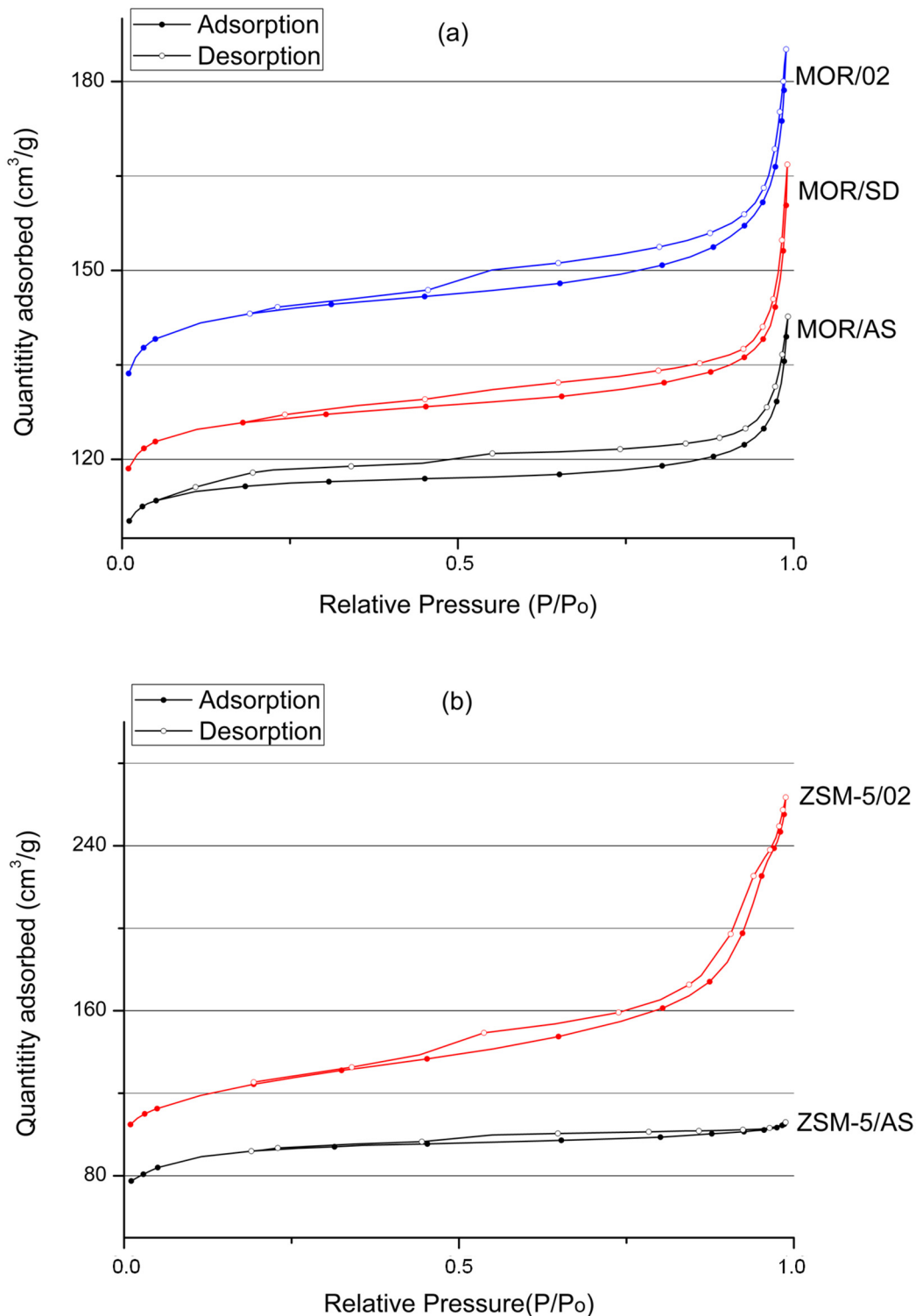


Figure 3. N₂ adsorption–desorption curves for (a) Mordenites: MOR/02 / MOR/SD, and MOR/AS. (b) ZSM-5: ZSM-4/02 and ZSM-5/AS.

The sample ZSM-5/02 presented an isotherm type IV with H3 hysteresis, indicating that the alkaline treatment efficiently formed mesopores. The sample ZSM-5/02 managed

to achieve a mesoporosity of 65% related to the total pore volume (Figure 3b). The textural properties are presented in Table 3.

Table 3. Textural analysis data of MOR and ZSM-5 catalysts.

Catalyst	Surface Area (m^2/g)		Pore Volume (cm^3/g)	
	BET	External (t-Plot)	Micropores (t-Plot)	Mesopores (BJH)
MOR/AS	344	20	0.168	0.043
MOR/02	426	39	0.201	0.072
MOR/SD	338	16	0.163	0.034
ZSM-5/AS	278	11	0.134	0.028
ZSM-5/02	383	153	0.100	0.253

The density of catalyst acid sites was obtained as quoted in the literature [36,37]. The maximum desorption temperatures and the relative number of strong/weak sites are shown in Table 4.

Table 4. Acid properties of catalysts obtained by TPD-NH₃.

Sample	Temperature (°C)	Total Acidity ($\mu\text{mol NH}_3/\text{g}$)	Weak/Medium Sites (%) *	Strong Sites (%) **
MOR/AS	288.7	511.8	2586	99.8
MOR/02	241.6	521.1	2207	71.4
MOR/SD	264.3	584.8	2093	66.3
ZSM-5/AS	-	-	-	-
ZSM-5/02	262.4	502.6	1965	68.7

* First desorption integration up to 400 °C; ** Integration of the second desorption above 400 °C.

The as-supplied MOR/AS mordenite showed high total acidity, almost entirely referring to weak acid sites (99.8%). The leaching process resulted in a decrease of 14.7% in the total acidity of the MOR/02 alkali-treated sample. A considerable increase in strong acidic sites was observed, reaching 28.6%. This is consistent with the behaviors reported in the literature [34,38].

The synthesized mordenite MOR/SD showed lower total acidity than MOR/02. However, the sample had the highest content of strong acid sites, equivalent to 33.7%. The alkali-treated ZSM-5/02 presented a well-defined strong and weak sites profile, with a 31.3% content of strong acid sites (Figure 4).

2.2. Waste Characterization

The post-consumer PE, PP, and PS plastics supplied for this study were characterized separately by DSC before mixing. The PE in the plastic mixture (PMix) presented a melting temperature of the crystals (T_m) of around 130 °C, characterizing the presence of high-density polyethylene (HDPE), which presents T_m in the range of 128–135 °C. Evaluating the cooling curve, it is possible to observe the main crystallization temperature (T_c), close to 120 °C, and a smaller peak, close to 110 °C, revealing the presence of polyethylene of different densities. The PP in the PMix had a T_m of 162 °C, which is about that as indicated for homopolymer PP, approximately 160 °C. In the cooling curve, there is a T_c with a major transition around 122 °C, a value next to that as reported in PP characterization works [39,40]. PS is an amorphous polymer, thus it exhibits no primary thermal transitions, T_m and T_c , but can be identified in the DSC curves by the glass transition temperature (T_g). A related secondary transition for this polymer is close to 100 °C [41]. PS in the PMix presented T_g at 97 °C, revealing the presence of this polymer and disclosing a melting peak at 126 °C, characteristic of the low-density class of polyethylene (LDPE or LLDPE). This suggests a PE contamination in the post-consumer PS sample, confirmed on the cooling curve, presenting a T_c at 120 °C.

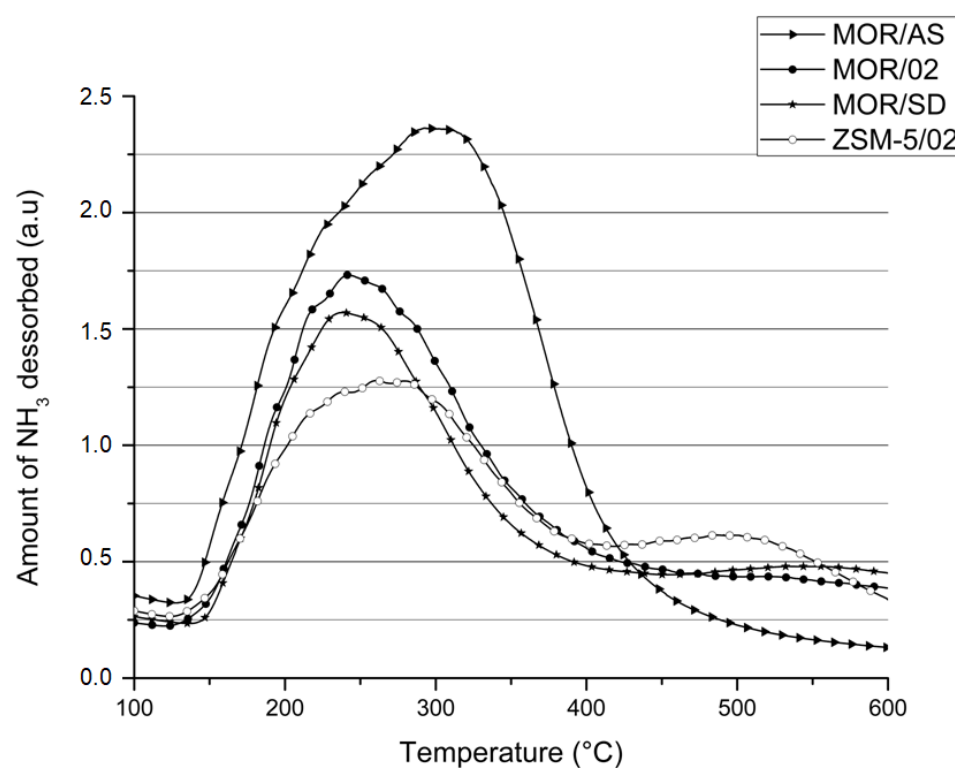


Figure 4. Curves of the temperature-programmed desorption of ammonia over the MOR and ZSM-5 samples.

2.3. TGA Pyrolysis

Figure 5 shows the TG and DTG curves associated with the thermal degradation of the PMix composed of 58.50% PE, 31.56% PP, and 9.94% PS incorporated with the different investigated zeolites catalysts.

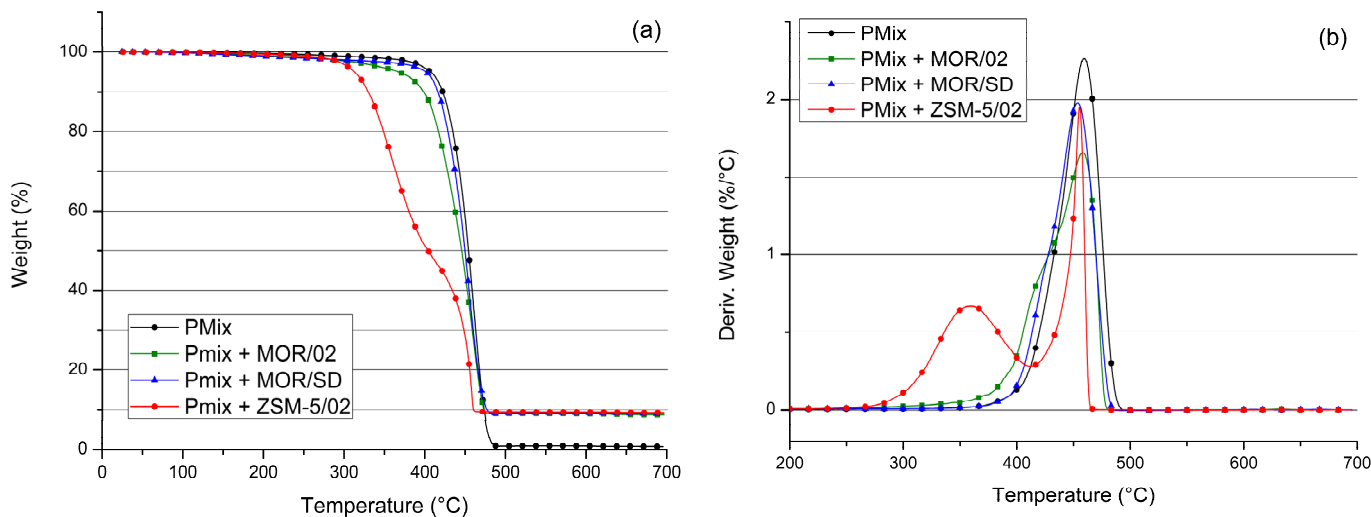


Figure 5. TG (a) and DTG (b) curves for PMix with catalysts.

Through the TG and DTG curves in Figure 5, it is possible to observe the influence of catalysts on the degradation of the plastic mixture, PMix. Both modified and synthesized mordenite exhibited a greater influence on the beginning of the degradation, $T_{10\%}$, decreasing these temperatures for PMix. It is also possible to observe the presence of a shoulder on the curve PMix with MOR/02, which indicates that the greater presence of mesopores contributed to an additional stage in the degradation of this material.

This behavior was observed with greater evidence for the pyrolysis of PMix with the catalyst ZSM-5/02, bearing a two-stage degradation curve, with decomposition temperatures close to 350 and 450 °C. This behavior of the ZSM-5 zeolite in plastic pyrolysis was also observed by Paula et al. [36]. The first degradation stage occurs due to mesopores on the catalyst's surface. The second one is related to smaller fragments accessing more internal acidic sites [42,43].

The crystallite size can mainly also influence the second degradation stage, since smaller crystals generate shorter diffusion paths [44,45], contributing to pyrolysis occurring at a lower degradation temperature ($T_{50\%}$), as observed for catalysts ZSM-5/SD and MOR/02.

Table 5 shows the initial degradation temperatures (T_{onset}), mass loss temperatures of 10% ($T_{10\%}$) and 50% ($T_{50\%}$), the temperature at the maximum thermal decomposition rate (T_{max}) for the PMix, and the percentage of residues determined by TGA. The influence on these parameters was more significant for the mordenite catalysts at the beginning of the degradation (decrease of T_{onset} and $T_{10\%}$), with little influence on T_{max} . In all TGA results, the percentage of the residue obtained was lower than 10%, which is the content of catalyst added, probably due to the catalyst thermal degradation.

Table 5. TGA results for the PMix sample with all catalysts.

Extrusions	T_{onset} (°C)	$T_{10\%}$ (°C)	$T_{50\%}$ (°C)	T_{Max} (°C)	Residue (%)
PMix	432.1	421.5	453.5	459.4	0.89
PMix + MOR/AS	429.6	422.9	456.0	461.0	9.62
PMix + MOR/02	417.4	398.3	445.1	458.2	8.99
PMix + MOR/SD	423.0	411.2	449.3	456.4	8.90
PMix + ZSM-5/02	387.1	329.5	403.7	455.4	9.40

2.4. Pyrolysis in Reactor

In principle, the PMix decomposition might be understood as a two-stage process beginning with thermal degradation followed by catalytic reforming. Table 6 presents the results of direct thermal pyrolysis of the PMix, and the catalytic pyrolysis of PMix added with mordenite and ZSM-5.

Table 6. Results of the non-catalytic PMix and catalytic pyrolysis.

Conversion (%)	Fraction C10-24 (%)	Fraction C > 24 (%)	Light Fraction (C10-24)		
			Aromatic (%)	Cyclic (%)	Aliphatic (%)
PMix	12.9 ± 2.0	69.7 ± 2.8	27.6 ± 2.8	26.1 ± 2.5	3.4 ± 0.9
PMix + MOR/02	14.3 ± 2.3	81.5 ± 1.9	18.5 ± 1.9	35.3 ± 1.9	4.3 ± 1.2
PMix + MOR/SD	14.5 ± 2.9	75.1 ± 2.1	24.9 ± 2.1	38.0 ± 2.9	3.7 ± 0.4
PMix + ZSM-5/02	49.2 ± 2.7	80.4 ± 1.3	22.4 ± 1.3	40.6 ± 0.6	7.1 ± 0.1

The PMix with mordenite catalysts, MOR/02 and MOR/SD, displayed a small conversion of 14.3% and 14.5%, respectively, compared with plain PMIX thermal pyrolysis (12.9%). Otherwise, for the catalyst ZSM-5/02, conversions were obtained around 49% and the expressive formation of gaseous products.

It is generally accepted for a zeolite that the higher the acidity, the greater the catalyst activity. This is because the cracking of polyolefins requires medium or strong acid sites for the reaction to occur via the carbene ion [45]. Still, other factors must be considered when zeolites of different families are compared since they have variations in their channel systems, pore structure, and textural properties [43,46]. Only a small conversion was found in mordenite compared to the plain PMix non-catalytic pyrolysis. Even though it exhibited total acidity higher than that of ZSM-5, mordenite also showed a lower mesopore content,

making it difficult for polymeric chains to access their acidic sites, leading to rapid deactivation. Alves et al. [32] reported that a greater mesoporosity decreases the shape selectivity of these catalysts, allowing larger chains to access internal acidic sites and contributing to an effective cracking of polymeric chains. The fact that the obtained mordenite did not achieve a significant mesoporosity content in their structures and unidimensional diffusion resulted in difficulty of moving larger molecules within its pores. As such, one molecule prevents another from passing through the mordenite pores. As a result, these mordenite catalysts become more susceptible to deactivation of their pores by the deposition of residual coke, or solid fraction originated during pyrolysis [21,47]. In addition, there may have been difficulties in cracking the composition of the PMix itself. Marcilla et al. [48] suggested that polymeric branches or the ends of the chains may have better access to active sites located on the surface of larger pores of zeolites, resulting in greater activities. According to this argument, the catalytic effect will be greater in polymers with higher branches or chain ends since the decomposition would contain many initiation points. As the PMix is formed mostly by HDPE, an almost entirely linear-chain polymer, the penetration of polymer chains in the catalyst's active sites may have been hampered, contributing to low conversions obtained in the pyrolysis.

The composition of the pyrolytic oils was determined by a semi-quantitative method, in which peaks in the homologous series in the interval of 5 to 50 min show the presence of C10 to C24 hydrocarbons [49]. The complete scans associated with the total ion chromatogram of the pyrolytic oil of thermal and catalytic pyrolysis are shown in Figure 6.

By evaluating the composition of the pyrolytic oil of the PMix in Figure 7, it is possible to observe that, even with the increase of light compounds in pyrolysis liquid products, the mordenite caused changes only in the composition of the light fraction. This is more significant for the synthetic MOR/SD, with a greater increase in the aromatics content shown in Figure 7b. It further confirms that this catalyst contributed to pyrolysis with its high acidity and specific area. However, due to the low mesoporous content, mordenite suffered rapid deactivation. Therefore, it is also possible that two-stage pyrolysis occurred in this case, with thermal degradation followed by catalytic reforming of the products. The present result demonstrated that mordenite might enhance its catalytic efficiency when modified to increase mesopore's amount and distribution. For the ZSM-5 catalyst, there was a greater formation of aromatic compounds, already predicted for this type of synthetic catalyst, with an increase of around 12%, accompanied by a reduction in aliphatic components.

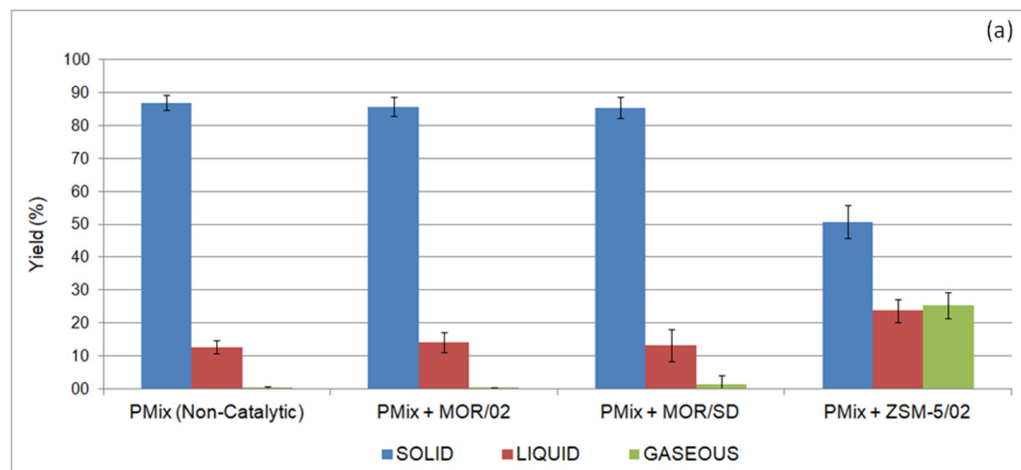


Figure 6. Cont.

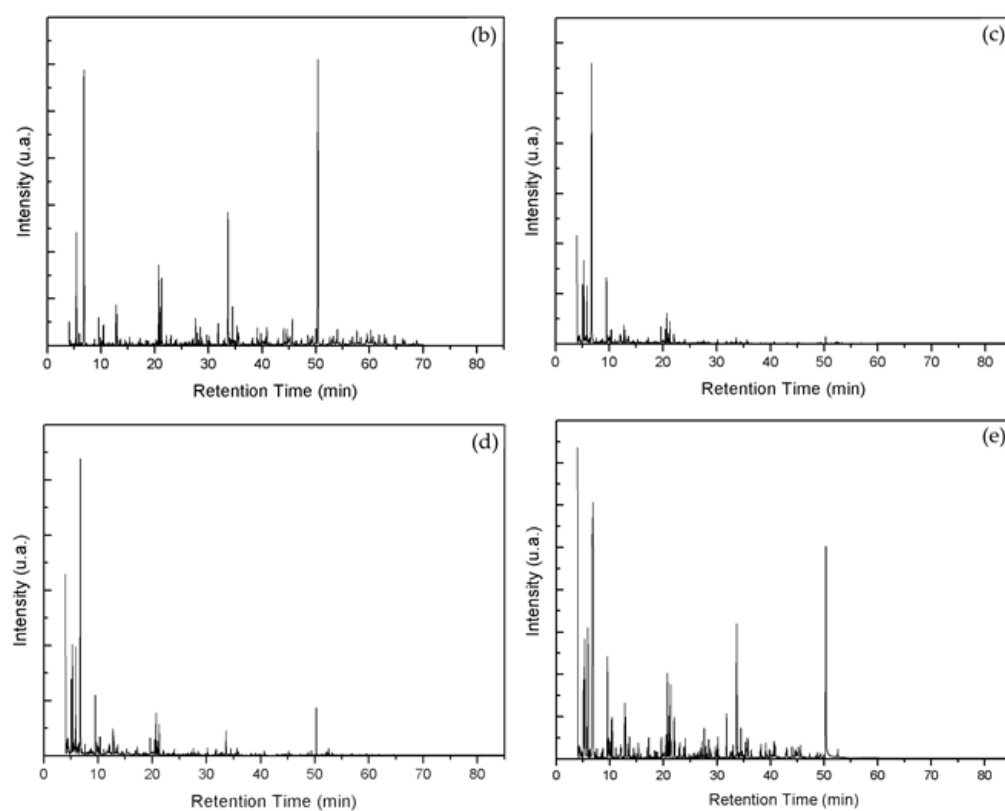


Figure 6. (a) Distribution of the pyrolysis products (gaseous, liquid, and solid fractions) of the PMix with different catalysts and the chromatograms of complete pyrolysis oil; (b) non-catalytic, (c) MOR/02, (d) MOR/SD, (e) ZSM-5/02.

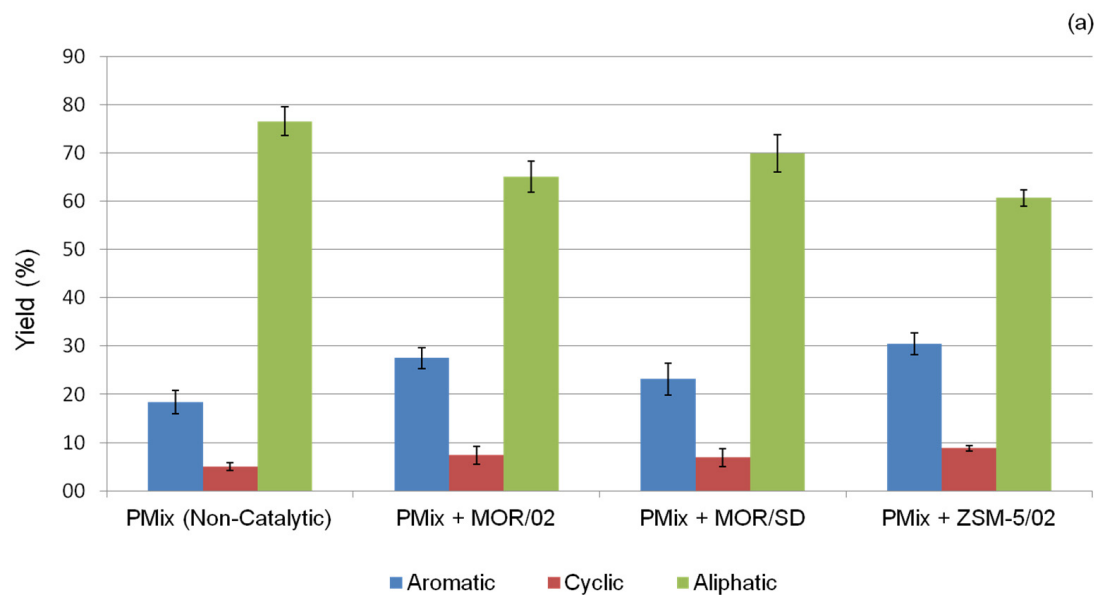


Figure 7. Cont.

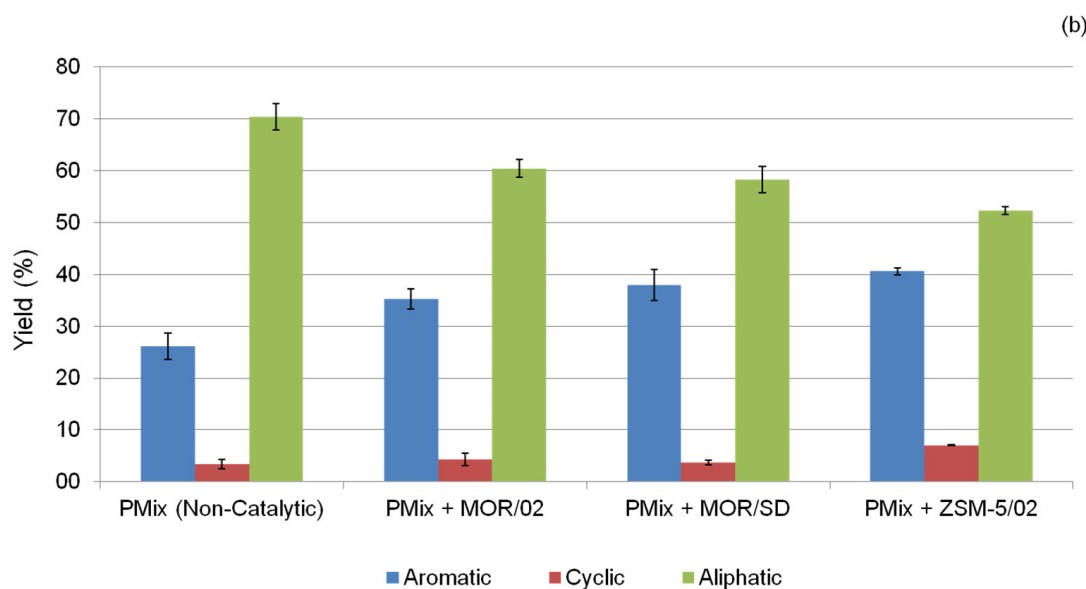


Figure 7. Composition of pyrolytic liquids in (a) aliphatic, cyclic and aromatic content in total product and (b) light fraction.

3. Discussion

The thermodynamic stability of the intermediate ion generated from a strong acid directly affects the formation of olefins in catalytic degradation [12,50]. This ion can follow the reaction routes (i) β fission or (ii) hydrogen transfer [51], with olefin production being enhanced when the intermediate ion favors β fission reactions. Otherwise, other products are generated. The stability of carbonium ions in acid catalysts will depend on their chemical properties. However, they are also affected by the pyrolysis conditions, the specific area, and the pore structure of the catalyst, related to its activity and selectivity [12,52].

Bimolecular secondary reactions are impaired in the case of mordenites with larger pores than ZSM-5. They have less stereo interconnection impediments, contributing to greater access to the interior pores. This characteristic promotes the formation of many alkenes as primary products. Thus, mordenite catalysts tend to generate more olefins than aromatics compared with ZSM-5 ones [42]. However, this is not what the present study found. An increased light aromatic fraction was generated when mordenite catalysts were added to PMix (Figure 7). As the mordenite presented an irregular pore size distribution, they may have contributed to secondary reactions occurring preferentially on the catalyst surface. According to Manos et al. [42] and Zhang et al. [12], this behavior can be justified by the difficulty of the intermediate cracking molecules in penetrating the catalyst's internal acid sites and impairing the subsequent cracking steps. Consequently, these molecules react more on the surface, favoring bimolecular secondary reactions and generating higher levels of aromatic compounds. The high acidity on the surface of the MOR/SD catalysts and the lower amount of mesopores may also have contributed to secondary reactions on the catalyst's surface.

Despite the lower conversion compared with ZSM-5/02, the present results disclose that mordenite modification in the direction of increasing the amount and regular distribution of mesopores might enhance its catalytic efficiency.

The formation of aromatics in catalytic pyrolysis of biomass and lignin with mordenite was also reported by Mihalcik et al. [53] and Kumar et al. [54], respectively. Kumar [55] noted that each zeolite's pore system, acidity, and pyrolysis temperature significantly affect product distribution. On the other hand, when comparing the performance of different zeolites as catalysts in biomass pyrolysis, Mihalcik et al. [53] found that the ZSM-5 was the most effective zeolite for the production of aromatic compounds, but also showed that the pore structure and channel size of the catalyst tend to affect the composition of the

pyrolysis product, coke formation and pore saturation, which directly affects the blocking and eventual deactivates the catalyst action.

As for the ZSM-5/02 catalyst, Figure 7 shows an increase in the content of aromatic and cyclic compounds, associated with a decrease in aliphatic ones, which revealed aromatic contents close to 40% and about 7% of cyclic and 52% of the aliphatic fraction. This behavior was expected since some studies with ZSM-5 catalysts reported high selectivity towards aromatics [12,51,54]. Seo et al. [52] identified the percentages of olefins, naphthene, and aromatics resulting from the thermal and catalytic pyrolysis of HDPE likewise at 450 °C as in our work, in a batch reactor. The percentages were 39% for olefins for thermal cracking, 18% for naphthene, and 0.68% for aromatics. The catalysts used were ZSM-5 and zeolite Y. For ZSM-5, the amounts were 16, 23, and 58% for olefins, naphthenes, and aromatics, respectively, while for the investigated zeolite Y, they were 79, 7, and 7%, respectively. The authors indicated that ZSM-5 favors secondary reactions in thermal pyrolysis, unlike zeolite Y.

Ratnasari et al. [51] investigated two-stage high-density polyethylene catalytic pyrolysis, thermal pyrolysis followed by catalytic with mesoporous MCM-41 catalysts followed by microporous ZSM-5. The results showed that a high oil product yield (83.15% by mass) was obtained from high-density polyethylene, with a highly aromatic product (95.85% by mass of oil) consisting of 97.72% by mass of hydrocarbons in the gasoline range, characteristic of the ZSM-5 catalyst. On the other hand, Li et al. [56], in their study on the catalytic pyrolysis of cellulose and low-density polyethylene, observed greater aromatic selectivity and the positive synergistic effect on co-pyrolysis, which increases the production of aromatics, decreases the formation of coke, and lowers the deactivation rate.

Hong et al. [55] investigated the effects of the pore size of the ZSM-5 catalyst on the generation of aromatic hydrocarbons in the co-pyrolysis of cellulose and polypropylene, observing that the formation of aromatic hydrocarbons are favored by the mesopores generated in the desilication of the ZSM-5. The authors indicated that this is because the opening of the catalyst pore allows the diffusion of large molecules in association with a decrease in stereo interconnectivity impediment. Their results corroborate the better performance found in the present investigated ZSM-5.

4. Materials and Methods

4.1. Materials

Post-consumer plastics were supplied by a company responsible for screening and sending materials for recycling in Rio de Janeiro, Brazil, selected after density separation, and classified as suitable for mechanical recycling. Three main types of municipal plastic wastes, classified as polyethylene (PE), polypropylene (PP), and polystyrene (PS), were used in concentrations equivalent to 58.50%, 31.56%, and 9.94%, respectively, for the formation of a plastic waste mixture, herein denoted as PMix. These plastic wastes were washed three times with ethanol and dried overnight. Subsequently, they were characterized by differential scanning calorimetry (DSC) in a TA Instruments model Q1000, (TA Inst, New Castle, DE, USA), where samples were heated from 25 to 200 °C with a heating rate of 10 °C/min and then cooled to room temperature. The data of the second heating run of the DSC analysis were considered. The two investigated precursor zeolites were the as-supplied commercial zeolite ZSM-5/AS, in ammoniacal form, donated by the Petrobras Research Center (CENPES) Rio de Janeiro, Brazil; and the mordenite zeolite CBV90A (MOR/AS) produced by PQ Corporation (Malvern, PA, USA), in its acid form. These zeolites were treated and used as catalysts for pyrolysis of the post-consumer PMix.

4.2. Chemical Treatment of Original Zeolites

The MOR/AS was subjected to the alkaline desilication process, according to Bertrand-Drira et al. [34], with a NaOH 0.2 M solution. After treatment, the solid phase was collected by centrifugation, washed with distilled water to pH 7, and dried overnight at 80 °C. Next, ion exchange was performed with ammonium chloride employing a 1 M solution of NH₄Cl

under reflux at 100 °C for 2 h. Next, the solid was centrifuged, washed with warm water three times, and oven-dried at 80 °C overnight. Finally, the product was calcined under a heating rate of 5 °C/min in static air at 550 °C for 12 h. The corresponding final sample was named MOR/02.

The ZSM-5/02 sample was obtained starting from ZSM-5/AS. The alkaline treatment was similar to that for mordenite, using 0.2 M NaOH solution, with a zeolite (g)/NaOH (mL) ratio of 0.008 at 75 °C for 30 min, as described in the literature [16,32]. In short, the zeolite was suspended in a 0.2 mol/L NaOH solution, and then the solid was separated by filtration and washed with deionized water until reaching neutral pH. Then, it was dried at 200 °C for 1 h. Next, ion exchange of the sample was performed with a 2 M NH₄Cl solution. The zeolite was then filtered, washed, and calcined at a rate of 5 °C/min under static air at 450 °C for 4.5 h.

4.3. Synthesis of Mordenite

The reaction for obtaining synthetic mordenite with the molar composition of 20SiO₂:1.0Al₂O₃: 4.0Na₂O was based on adaptations of Santos et al. [57], using the route of soft template synthesis employing a cationic surfactant. A solution containing 0.94 g of sodium hydroxide in 30 mL of distilled water was placed under mechanical stirring, to which 3.7 g of the surfactant cetyltrimethylammonium bromide (CTABr) was added. Subsequently, 0.95 g of sodium aluminate (NaAlO₂) was added, stirring for 10 min. Finally, 5.61 g of hydrophilic fumed silica, Aerosil 200, was slowly added, and after the homogenization period, the formed mass was dried in an oven at 100 °C for 24 h. Subsequently, the dry solid was sieved. Then, about 2 g of that solid was placed on Teflon support, and 60 mL of distilled water was added to the reactor to avoid contact between the solid and water. After, the ion exchange was carried out, in which for every 2 g of mordenite obtained, a solution was prepared with 0.99 g of NH₄Cl in 18.80 mL of distilled water and kept in reflux at 100 °C for 2 h. Next, the solid was centrifuged, washed three times with warm water, and oven-dried at 80 °C overnight. Finally, the solid was calcined under a heating rate of 5 °C/min in static air at 550 °C for 12 h and identified as synthetic-developed MOR/SD.

4.4. Catalyst Characterization

The crystalline phases of the samples were determined by X-ray diffraction (XRD) on a Rigaku Miniflex diffractometer (The Woodlands, TX, USA), using Cu-K α radiation ($\lambda = 0.1542$ nm) at 30 kV and 15 mA. XRD data were recorded in a 2 θ range from 5 to 50° with an angular step of 0.05° and a counting time of 1°(2 θ)/min. The average crystal size was calculated by the Scherrer formula using XRD data according to Equation (1):

$$D_{hkl} = \frac{k\lambda}{\beta \cos \cos \theta} \quad (1)$$

where D is the size of the crystallite in the direction perpendicular to the planes analyzed, hkl are the Miller indices of these planes, k is a numerical factor often referred to as the crystallite shape ($k = 0.9$), λ is the X-ray wavelength (nm), β is the width at half-height of the peak after correction for intrinsic, instrumental line extension using the FIT2K software (Free Software Foundation Inc., Boston, MA, USA). Angles must be in radians, and θ is the Bragg angle, i.e., the maximum peak angle [28]. Anisotropic broadening due to non-isometric crystallite shape was neglected.

Textural properties were determined on a Micromeritics ASAP 2020 ASTM 2020 nitrogen gas adsorption analyzer (Norcross, GA, USA), measured at -196 °C, with automatic degassing. Before analysis, the samples were treated at 300 °C for 12 h under vacuum. The surface area was estimated by the Brunauer–Emmett–Teller (BET) equation. Total pore volume was determined from nitrogen adsorbed at P/P₀ = 0.98, microporous volume and external surface area were determined by the t-plot method, the mesoporosity was obtained by the Barrett–Joyner–Halenda (BJH) method.

The Halsey thickness equation with Faas correction was used to calculate the thickness (t) of the layer adsorbed on the pore walls to a given relative pressure. External surface area and micropore volume were determined by applying the t-plot method. In this method, the adsorbed layer thickness (t) of N_2 was calculated with the Harkins-Jura equation.

All analyses of the composition of the catalysts were made using their powder form. Energy Dispersive X-ray Fluorescence Spectrometry (ED-XRF) was performed on a Shimadzu spectrometer model 720 (Kyoto, Japan), under vacuum, in which the results were expressed as mass% of the elements. The molar amounts of Si and Al in the samples were obtained by dividing the mass% of Si and Al by the respective molar mass, and the bulk Si/Al molar ratio was calculated [16]. The zeolite composition was also determined by dispersive energy spectrometry coupled with scanning electron microscopy (SEM-EDS) that analyzes the localized elemental composition. The measurements were performed at three different points, and the averages of the amounts of Si and Al present in the points of the evaluated surface were calculated.

The framework's Si/Al molar ratio and the extra-framework Al (EFAL) content of the studied zeolites were determined by solid-state nuclear magnetic resonance (NMR) of ^{29}Si and ^{27}Al . Both ^{29}Si and ^{27}Al NMR spectra were obtained in a Bruker Avance 400 spectrometer (MA, USA) at a resonant frequency of 79.2 MHz, while ^{27}Al MAS NMR spectra were acquired at 103.9 MHz on the same spectrometer. The Si/Al molar ratio in the structure was calculated from the ^{29}Si MAS NMR spectra using Equation (2):

$$Si/Al_{NMR \ 29Si} = \frac{\sum_{n=0}^4 I_{Si(nAl)}}{\sum_{n=0}^4 0.25nI_{Si(nAl)}} \quad (2)$$

where n is the number of Al atoms in the second Si coordination sphere, and I is the peak intensity corresponding to the Si environment (nAl).

Two peaks are expected in the ^{27}Al MAS NMR spectra, the first with a chemical shift close to 60 ppm, corresponding to tetrahedral Al atom, and the second at around 0 ppm, octahedral Al (EFAL% = 100% – Al tetra%).

The total acidity and strength distribution of the acid sites present in the catalysts were evaluated by the temperature-programmed desorption (TPD-NH₃) technique in a Pfeiffer PrismaPlus quadrupole mass spectrometer model QMG220 (Asslar, Germany), as described by Paula et al. [36]. Briefly, 120 mg of sample was pretreated in a U-shaped quartz tubular reactor (heating to 600 °C, helium flow of 30 mL/min). The sample was cooled to 100 °C, and the chemisorption process was initiated. Adsorption step: passing through the sample a 30 mL/min flow of 5% molar NH₃ in He until saturated. Then, a stream of pure He was passed at the same flow to remove the physisorbed ammonia. This cycle was repeated, and the total acidity was calculated by the difference between the areas obtained in the two adsorption peaks. Desorption process: at 100 °C to 600 °C at a heating rate of 10 °C/min under the same He flow. The amount of NH₃ desorbed x temperature was measured through the mass spectrometer.

4.5. Pyrolysis of Plastic Waste

4.5.1. TGA Pyrolysis

For the thermogravimetric analysis (TGA) of the pyrolysis characteristics, the plastic mixture (PMix) was extruded either plain or mixed with the catalysts for homogenization of the samples using a Haake Minilab (Agawam, MA, USA), double screw mini-extruder at 60 RPM for 7 min at 180 °C, 10% by mass catalyst content. Then, pyrolysis in TGA was carried out in triplicate in a TA Instruments Q500 equipment (New Castle, DE, USA), with a heating rate of 10 °C/min to 700 °C under a nitrogen atmosphere [9].

4.5.2. Pyrolysis in Pyrolysis Reactor

Pyrolysis was performed in triplicate under a nitrogen atmosphere at 450 °C for 15 min at a 30 mL/min flow rate. The pyrolysis system consists of a fixed bed unit with

a stainless-steel tubular reactor and a vertical electric oven. To carry out the experiment, approximately 1 g of the plastic mixture was weighed, and 0.1 g of catalyst was previously mixed. The preparation of the reactors was initially carried out by weighing about 0.3 g of glass wool, which had the function of composing the reactor bed, in order to leave the material to be pyrolyzed in the central zone of the reactor and to help maintain the residual pyrolysis solid inside during the process. This already heavy glass wool wad was divided into two parts. The first part of the glass wool was inserted at the end of the reactor, and later, the plastic–catalyst mixture was inserted into the reactor over this wool. Finally, another part of the glass wool was inserted into the reactor.

The yield was determined by gravimetric analysis of the pyrolytic residue (solid fraction) and pyrolytic oil (liquid fraction), while the gas yield (gaseous fraction) was determined by difference [58]. The liquid fractions were dissolved in n-hexane and analyzed by HRGC–MS, Scion 456 HRGC-TQ, Bruker (City, MA, USA). This device has a 30 m × 0.25 mm, coated with a 0.1 µm thick 5% phenylmethyl polysiloxane (BR-5) film, with a heating ramp up to 300 °C, at a heating rate of 10 °C/min, maintained for 25 min.

A semi-quantitative methodology was used to determine the percentages of the peaks for light and heavy compounds concerning the area of the total ion chromatogram. The yields of aromatic, linear, and cyclic compounds were determined as described by Milato et al. [49] and Faillace et al. [59]. In brief, aromatic, linear, and cyclic yields were determined by reconstructed ion chromatogram using *m/z* 77, 85, and 191, respectively. Data were processed by the MS Data Review® program (V. 8.0, Chemical Analysis, Bruker, City, State if Canada/USA, Country).

5. Conclusions

In this work, for the first time, the catalytic activity of the developed synthetic and chemically-modified mordenites was compared to the modified ZSM-5 zeolite as catalysts in the pyrolysis of a real mixture of plastic waste. With alkaline treatment and calcination, a low content of mesoporosity in the mordenite catalyst structures was obtained. However, with its high surface acidity, mordenite catalysts contributed to a small increase of light compounds (C10-C24) in pyrolysis liquid products. Furthermore, this class of catalysts proved to be very susceptible to deactivation, resulting in low conversion rates. It is suggested that this may be related to their monodimensional channel systems and the low mesoporosity that hindered the access of polymer chains to their innermost active sites. Another indication that cracking reactions occurred mainly on the surface of mordenite was the increased number of aromatic molecules in the liquid pyrolysis products. Indeed, surface reactions favor bimolecular secondary reactions, generating more aromatic compounds and reaching 82% of light fraction (C10-C24) hydrocarbons. Despite the lower catalytic conversion compared with ZSM-5, these results show that mordenite has potential in the pyrolysis of urban plastic wastes. Indeed, if modified to increase the mesopore amount and distribution, mordenite might enhance its catalytic activity. The alkaline-treated catalyst ZSM-5 resulted in a better catalytic performance in the pyrolysis than mordenite by significantly decreasing the degradation temperature of the mixture of plastic waste in association with bimodal thermogravimetric curves. Likewise, in the reactor pyrolysis, the performance of the ZSM-5 catalyst was also superior, with greater conversion rates of about 49% for the liquid and gas fractions.

Supplementary Materials: The following supporting information can be downloaded at: <https://www.mdpi.com/article/10.3390/chemistry4020023/s1>; Figure S1: ^{29}Si NMR spectrum of MOR/02; Figure S2: ^{29}Si NMR spectrum of MOR/SD; Figure S3: ^{29}Si NMR spectrum of ZSM-5/02; Figure S4: ^{27}Al NMR spectrum of MOR/02; Figure S5: ^{27}Al NMR spectrum of MOR/SD; Figure S6: ^{27}Al NMR spectrum of ZSM-5/02; Figure S7: Diffractogram of zeolites ZSM-5 and MOR. Available in Database of zeolite Structure (CIF files).

Author Contributions: Conceptualization, T.P.P. and M.d.F.V.M.; methodology, T.P.P. and M.R.d.C.M.; validation, T.P.P., M.d.F.V.M., M.S.O. and S.N.M.; formal analysis, M.d.F.V.M. and S.N.M.; investi-

gation, T.P.P. and M.R.d.C.M.; resources, T.P.P. and S.N.M.; data curation, T.P.P., M.S.O. and S.N.M.; writing—original draft preparation, T.P.P., M.R.d.C.M. and M.d.F.V.M.; writing—review and editing, M.S.O. and S.N.M.; supervision, M.d.F.V.M. and S.N.M.; project administration, T.P.P., M.d.F.V.M. and S.N.M.; funding acquisition, T.P.P. and M.d.F.V.M. All authors have read and agreed to the published version of the manuscript.

Funding: This research was funded by Chagas Filho de Amparo à Pesquisa do Estado do Rio de Janeiro (FAPERJ), Coordenação de Aperfeiçoamento de Pessoal de Nível Superior (CAPES) and Conselho Nacional de Desenvolvimento Científico e Tecnológico (CNPq).

Institutional Review Board Statement: Not applicable.

Informed Consent Statement: Not applicable.

Data Availability Statement: All the relevant data used in this study have been provided in the form of figures and tables in the published article, and all data provided in the present manuscript are available to whom it may concern.

Acknowledgments: The authors would like to acknowledge Chagas Filho de Amparo à Pesquisa do Estado do Rio de Janeiro (FAPERJ), Ministry of Science and Technology of the Brazil and the support of Coordenação de Aperfeiçoamento de Pessoal de Nível Superior (CAPES), Conselho Nacional de Desenvolvimento Científico e Tecnológico (CNPq), as well as Institute of Macromolecules Eloisa Mano for providing the research facilities.

Conflicts of Interest: The authors declare no conflict of interest.

References

1. Kasar, P.; Sharma, D.K.; Ahmaruzzaman, M. Thermal and catalytic decomposition of waste plastics and its co-processing with petroleum residue through pyrolysis process. *J. Clean. Prod.* **2020**, *265*, 121639. [[CrossRef](#)]
2. Melaré, A.V.S.; González, S.M.; Faceli, K.; Casadei, V. Technologies and decision support systems to aid solid-waste management: A systematic review. *Waste Manag.* **2017**, *59*, 567–584. [[CrossRef](#)] [[PubMed](#)]
3. Fivga, A.; Dimitriou, I. Pyrolysis of plastic waste for production of heavy fuel substitute: A techno-economic assessment. *Energy* **2018**, *149*, 865–874. [[CrossRef](#)]
4. Geyer, R.; Jambeck, J.R.; Law, K.L. Production, use, and fate of all plastics ever made. *Sci. Adv.* **2017**, *3*, 25–29. [[CrossRef](#)] [[PubMed](#)]
5. Moya, D.; Aldás, C.; López, G.; Kaparaju, P. Municipal solid waste as a valuable renewable energy resource: A worldwide opportunity of energy recovery by using Waste-To-Energy Technologies. *Energy Procedia* **2017**, *134*, 286–295. [[CrossRef](#)]
6. Zhang, Y.; Duan, D.; Lei, H.; Villota, E.; Ruan, R. Jet fuel production from waste plastics via catalytic pyrolysis with activated carbons. *Appl. Energy* **2019**, *251*, 11337. [[CrossRef](#)]
7. Kaimal, V.K.; Vijayabalan, P. A study on synthesis of energy fuel from waste plastic and assessment of its potential as an alternative fuel for diesel engines. *Waste Manag.* **2016**, *51*, 91–96. [[CrossRef](#)]
8. Kumar, S.; Panda, A.K.; Singh, R.K. A review on tertiary recycling of high-density polyethylene to fuel. *Resour. Conserv. Recycl.* **2011**, *55*, 893–910. [[CrossRef](#)]
9. Budsareechai, S.; Hunt, A.J.; Ngernyen, Y. Catalytic pyrolysis of plastic waste for the production of liquid fuels for engines. *RSC Adv.* **2019**, *9*, 5844–5857. [[CrossRef](#)]
10. Li, K.; Lei, J.; Yuan, G.; Weerachanchai, P.; Wang, J.Y.; Zhao, J.; Yang, Y. Fe-, Ti-, Zr- and Al-pillared clays for efficient catalytic pyrolysis of mixed plastics. *Chem. Eng. J.* **2017**, *317*, 800–809. [[CrossRef](#)]
11. Obali, Z.; Sezgi, N.A.; Doğu, T. Catalytic degradation of polypropylene over alumina loaded mesoporous catalysts. *Chem. Eng. J.* **2012**, *207–208*, 421–425. [[CrossRef](#)]
12. Zhang, X.; Lei, H.; Yadavalli, G.; Zhu, L.; Wei, Y.; Liu, Y. Gasoline-range hydrocarbons produced from microwave-induced pyrolysis of low-density polyethylene over ZSM-5. *Fuel* **2015**, *144*, 33–42. [[CrossRef](#)]
13. Miandad, R.; Barakat, M.A.; Aburazzaiza, A.S.; Rehan, M.; Ismail, I.M.I.; Nizami, A.S. Effect of plastic waste types on pyrolysis liquid oil. *Int. Biodeterior. Biodegrad.* **2017**, *119*, 239–252. [[CrossRef](#)]
14. Li, J.; Li, X.; Zhou, G.; Wang, W.; Wang, C.; Komarneni, S.; Wang, Y. Catalytic fast pyrolysis of biomass with mesoporous ZSM-5 zeolites prepared by desilication with NaOH solutions. *Appl. Catal. A Gen.* **2014**, *470*, 115–122. [[CrossRef](#)]
15. Djinović, P.; Tomše, T.; Grdadolnik, J.; Božić, Š.; Erjavec, B.; Zabilskiy, M.; Pintar, A. Natural aluminosilicates for catalytic depolymerization of polyethylene to produce liquid fuel-grade hydrocarbons and low olefins. *Catal. Today* **2015**, *258*, 648–659. [[CrossRef](#)]
16. Santos, B.P.S.; Almeida, D.; Maria de Fatima, V.M.; Henriques, C.A. Petrochemical feedstock from pyrolysis of waste polyethylene and polypropylene using different catalysts. *Fuel* **2018**, *215*, 515–521. [[CrossRef](#)]
17. Meier, W.M. The crystal structure of mordenite (ptilolite). *Z. Kristallogr.* **1961**, *115*, 439–450. [[CrossRef](#)]

18. Li, X.F.; Prins, R.; Van Bokhoven, J.A. Synthesis and characterization of mesoporous mordenite. *J. Catal.* **2009**, *262*, 257–265. [[CrossRef](#)]
19. Gu, F.N.; Wei, F.; Yang, J.Y.; Lin, N.; Lin, W.G.; Wang, Y.; Zhu, J.H. New strategy to synthesis of hierarchical mesoporous zeolites. *Chem. Mater.* **2010**, *22*, 2442–2450. [[CrossRef](#)]
20. Cui, Y.; Yao, H.; Gao, B.; Qin, Y.; Zhang, S.; Yang, B.; He, C.; Xu, B.; Hou, J. Fine-Tuned Photoactive and Interconnection Layers for Achieving over 13% Efficiency in a Fullerene-Free Tandem Organic Solar Cell. *J. Am. Chem. Soc.* **2017**, *139*, 7302–7309. [[CrossRef](#)]
21. Galarneau, A.; Villemot, F.; Rodriguez, J.; Fajula, F.; Coasne, B. Validity of the t-plot method to assess microporosity in hierarchical micro/mesoporous materials. *Langmuir* **2014**, *30*, 13266–13274. [[CrossRef](#)] [[PubMed](#)]
22. Liu, Z.; Yi, X.; Wang, G.; Tang, X.; Li, G.; Huang, L.; Zheng, A. Roles of 8-ring and 12-ring channels in mordenite for carbonylation reaction: From the perspective of molecular adsorption and diffusion. *J. Catal.* **2019**, *369*, 335–344. [[CrossRef](#)]
23. Chaouati, N.; Soualah, A.; Chater, M.; Pinard, L. Beneficial changes in coke properties with alkaline treatment on aluminum-rich mordenite. *J. Catal.* **2017**, *353*, 28–36. [[CrossRef](#)]
24. ABIPLAST. *Brazilian Plastic Processed and Recycling Industry—Profile 2018*; Brazilian Plast Ind Assoc: São Paulo, Brazil, 2018; p. 47.
25. Paixão, V.; Carvalho, A.P.; Rocha, J.; Fernandes, A.; Martins, A. Modification of MOR by desilication treatments: Structural, textural and acidic characterization. *Microporous Mesoporous Mater.* **2010**, *131*, 350–357. [[CrossRef](#)]
26. Wang, Q.; Xu, S.; Chen, J.; Wei, Y.; Li, J.; Fan, D.; Yu, Z.; Qi, Y.; He, Y.; Xu, S.; et al. Synthesis of mesoporous ZSM-5 catalysts using different mesogenous templates and their application in methanol conversion for enhanced catalyst lifespan. *RSC Adv.* **2014**, *4*, 21479–21491. [[CrossRef](#)]
27. Schallmoser, S.; Ikuno, T.; Wagenhofer, M.F.; Kolenbach, R.; Haller, G.L.; Sanchez-Sanchez, M.; Lercher, J.A. Impact of the local environment of Brønsted acid sites in ZSM-5 on the catalytic activity in n-pentane cracking. *J. Catal.* **2014**, *316*, 93–102. [[CrossRef](#)]
28. Sadowska, K.; Wach, A.; Olejniczak, Z.; Kuśtrowski, P.; Datka, J. Hierarchic zeolites: Zeolite ZSM-5 desilicated with NaOH and NaOH/tetrabutylamine hydroxide. *Microporous Mesoporous Mater.* **2013**, *167*, 82–88. [[CrossRef](#)]
29. Smail, H.; Shareef, K.; Ramli, Z. Synthesis of Mesoporous Mordenite Zeolite by Different Natural Raw Materials. *Aust. J. Basic Appl. Sci.* **2017**, *11*, 27–34.
30. Song, Z.; Takahashi, A.; Mimura, N.; Fujitani, T. Production of propylene from ethanol over ZSM-5 zeolites. *Catal. Lett.* **2009**, *131*, 364–369. [[CrossRef](#)]
31. Khatamian, M.; Irani, M. Preparation and characterization of nanosized ZSM-5 zeolite using kaolin and investigation of kaolin content, crystallization time and temperature changes on the size and crystallinity of products. *J. Iran. Chem. Soc.* **2009**, *6*, 187–194. [[CrossRef](#)]
32. Alves, I.C.; Nascimento, T.L.P.M.; Veloso, C.O.; Zötin, F.M.Z.; Henriquez, C.A. Mesopore generation in ZSM-5 zeolites and their effects on conversion of ethanol to olefins. *Quim. Nova* **2012**, *35*, 1554–1559. [[CrossRef](#)]
33. Frantz, T.S.; Ruiz, W.A.; Rosa, C.A.; Mortola, V.B. Synthesis of ZSM-5 with high sodium content for CO₂ adsorption. *Microporous Mesoporous Mater.* **2016**, *222*, 209–217. [[CrossRef](#)]
34. Bertrand-Drira, C.; Cheng, X.; Cacciaguerra, T.; Trens, P.; Melinte, G.; Ersen, O.; Minoux, D.; Finiels, A.; Fajula, F.; Gerardin, C. Mesoporous mordenites obtained by desilication: Mechanistic considerations and evaluation in catalytic oligomerization of pentene. *Microporous Mesoporous Mater.* **2015**, *213*, 142–149. [[CrossRef](#)]
35. Bohström, Z.; Lillerud, K.P. Preparation of chabazite with mesopores templated from a cationic polymer. *Microporous Mesoporous Mater.* **2018**, *271*, 295–300. [[CrossRef](#)]
36. Paula, T.P.; Marques, M.F.V.; Costa Marques, M.R. Influence of mesoporous structure ZSM-5 zeolite on the degradation of Urban plastics waste. *J. Therm. Anal. Calorim.* **2019**, *138*, 3689–3699. [[CrossRef](#)]
37. Jin, H.; Ansari, M.B.; Jeong, E.Y.; Park, S.E. Effect of mesoporosity on selective benzylolation of aromatics with benzyl alcohol over mesoporous ZSM-5. *J. Catal.* **2012**, *291*, 55–62. [[CrossRef](#)]
38. Ivanova, I.I.; Kuznetsov, A.S.; Ponomareva, O.A.; Yuschenko, V.V.; Knyazeva, E.E. Micro/mesoporous catalysts obtained by recrystallization of mordenite. *Stud. Surf. Sci Catal.* **2005**, *158*, 121–128.
39. Ramos, S.; Carvalho, L.; Spieth, E.; Rivadula, R. Efeitos da estabilização do Polipropileno nas propriedades térmicas, mecânicas e termomecânicas de compósitos de Polipropileno/Atapulgita. *Polímeros Ciência e Tecnol.* **1993**, *3*, 26–31.
40. Líbano, E.V.D.G.; Visconde, L.L.Y.; Pacheco, É.B.A.V. Propriedades Térmicas de Compósitos de Polipropileno e Bentonita Organofílica. *Polímeros* **2012**, *22*, 430–435. [[CrossRef](#)]
41. Mark, J.E. *Polymer Data Handbook*, 3rd ed.; Oxford University Press: Oxford, UK, 1999; pp. 829–838.
42. Manos, G.; Garforth, A.; Dwyer, J. Catalytic degradation of high-density polyethylene over different zeolitic structures. *Ind. Eng. Chem. Res.* **2000**, *39*, 1198–1202. [[CrossRef](#)]
43. Marcilla, A.; Beltrán, M.I.; Hernández, F.; Navarro, R. HZSM5 and HUSY deactivation during the catalytic pyrolysis of polyethylene. *Appl. Catal A Gen.* **2004**, *278*, 37–43. [[CrossRef](#)]
44. Aguado, J.; Serrano, D.P.; Escola, J.M.; Peral, A. Catalytic cracking of polyethylene over zeolite mordenite with enhanced textural properties. *J. Anal. Appl. Pyrolysis* **2009**, *85*, 352–358. [[CrossRef](#)]
45. Kim, K.; Ryoo, R.; Jang, H.D.; Choi, M. Spatial distribution, strength, and dealumination behavior of acid sites in nanocrystalline MFI zeolites and their catalytic consequences. *J. Catal.* **2012**, *288*, 115–123. [[CrossRef](#)]
46. Aguado, J.; Serrano, D.P.; Miguel, G.S.; Escola, J.M.; Rodríguez, J.M. Catalytic activity of zeolitic and mesostructured catalysts in the cracking of pure and waste polyolefins. *J. Anal. Appl. Pyrolysis* **2007**, *78*, 153–161. [[CrossRef](#)]

47. Chaouati, N.; Soualah, A.; Chater, M.; Tarighi, M.; Pinard, L. Mechanisms of coke growth on mordenite zeolite. *J. Catal.* **2016**, *344*, 354–364. [[CrossRef](#)]
48. Marcilla, A.; Beltrán, M.I.; Navarro, R. Effect of regeneration temperature and time on the activity of HUSY and HZSM5 zeolites during the catalytic pyrolysis of polyethylene. *J. Anal. Appl. Pyrolysis* **2005**, *74*, 361–369. [[CrossRef](#)]
49. Milato, J.V.; França, R.J.; Marques, M.R.C. Pyrolysis of oil sludge from the offshore petroleum industry: Influence of different mesoporous zeolites catalysts to obtain paraffinic products. *Environ. Technol.* **2019**, *42*, 1013–1022. [[CrossRef](#)]
50. Panda, A.K.; Singh, R.K.; Mishra, D.K. Thermolysis of waste plastics to liquid fuel. A suitable method for plastic waste management and manufacture of value-added products—A world prospective. *Renew. Sustain. Energy Rev.* **2010**, *14*, 233–248. [[CrossRef](#)]
51. Ratnasari, D.K.; Nahil, M.A.; Williams, P.T. Catalytic pyrolysis of waste plastics using staged catalysis for production of gasoline range hydrocarbon oils. *J. Anal. Appl. Pyrolysis* **2017**, *124*, 631–637. [[CrossRef](#)]
52. Seo, Y.; Lee, K.; Shin, D. Investigation of catalytic degradation of high-density polyethylene by hydrocarbon group type analysis. *J. Anal. Appl. Pyrolysis* **2003**, *70*, 383–398. [[CrossRef](#)]
53. Mihalcik, D.J.; Mullen, C.A.; Boateng, A.A. Screening acidic zeolites for catalytic fast pyrolysis of biomass and its components. *J. Anal. Appl. Pyrolysis* **2011**, *92*, 224–232. [[CrossRef](#)]
54. Kumar, A.; Kumar, A.; Kumar, J.; Bhaskar, T. Catalytic pyrolysis of soda lignin over zeolites using pyrolysis gas chromatography-mass spectrometry. *Bioresour. Technol.* **2019**, *291*, 121822. [[CrossRef](#)] [[PubMed](#)]
55. Hong, Y.; Lee, Y.; Rezaei, P.S.; Kim, B.S.; Jeon, J.K.; Jae, J.; Jung, S.C.; Kim, S.C.; Park, Y.K. In-situ catalytic copyrolysis of cellulose and polypropylene over desilicated ZSM-5. *Catal. Today* **2017**, *293*, 151–158. [[CrossRef](#)]
56. Li, X.; Zhang, H.; Li, J.; Su, L.; Zuo, J.; Komarneni, S.; Wang, Y. Improving the aromatic production in catalytic fast pyrolysis of cellulose by co-feeding low-density polyethylene. *Appl. Catal. A Gen.* **2013**, *455*, 114–121. [[CrossRef](#)]
57. Santos, B.P.S.; Almeida, N.C.; Santos, I.S.; Marques, M.F.V.; Fernandes, L.D. Synthesis and Characterization of Mesoporous Mordenite Zeolite Using Soft Templates. *Catal. Lett.* **2018**, *148*, 1870–1878. [[CrossRef](#)]
58. Joppert, N.; Silva, A.A.; Marques, M.R.C. Enhanced diesel fuel fraction from waste high-density polyethylene and heavy gas oil pyrolysis using factorial design methodology. *Waste Manag.* **2015**, *36*, 166–176. [[CrossRef](#)]
59. Faillace, J.G.; Melo, C.F.; Souza, S.P.L.; Marques, M.R.C. Production of light hydrocarbons from pyrolysis of heavy gas oil and high-density polyethylene using pillared clays as catalysts. *J. Anal. Appl. Pyrolysis* **2017**, *126*, 70–76. [[CrossRef](#)]